Title
Second harmonic generation as a probe of broken mirror symmetry

Journal
Physical Review B, 101(24)

ISSN
2469-9950

Authors
Fichera, Bryan T
Kogar, Anshul
Ye, Linda
et al.

Publication Date
2020-06-01

DOI
10.1103/physrevb.101.241106

Peer reviewed

Second Harmonic Generation as a Probe of Broken Mirror Symmetry in a Charge Density Wave Transition

Bryan T. Fichera,[1] Anshul Kogar,[1] Linda Ye,[1] Bilal Göcke,[1,2] Alfred Zong,[1] Joseph G. Checkelsky,[1] and Nuh Gedik[1,*]

[1] *Department of Physics, Massachusetts Institute of Technology, Cambridge, Massachusetts 02139, USA*
[2] *Technical Chemistry I and Center for Nanointegration Duisburg-Essen (CENIDE), University of Duisburg-Essen, 45141 Essen, Germany*

(Dated: October 8, 2019)

The notion of spontaneous symmetry breaking has been used to describe phase transitions in a variety of physical systems. In crystalline solids, the breaking of certain symmetries, such as mirror symmetry, is difficult to detect unambiguously. Using $1T$-TaS_2, we demonstrate here that rotational-anisotropy second harmonic generation (RA-SHG) is a sensitive technique for the detection of broken mirror symmetry. We find that RA-SHG can differentiate between mirror symmetry-broken structures of opposite planar chirality. We are also able to identify a binary indicator of broken mirror symmetry, as well as an indicator of the sense of the planar chirality. Lastly, we find evidence for bulk mirror symmetry-breaking in the incommensurate charge density wave phase of $1T$-TaS_2. Our results pave the way for RA-SHG to probe candidate materials where broken mirror symmetry may play a pivotal role.

In condensed matter systems, phases are often classified by the symmetries that they break. Identifying these symmetries enables one to understand a system's order parameter, collective excitations, topological defects, and allowable topological indices [1, 2]. Together, these attributes ultimately allow one to predict how a material will respond to external perturbations like electromagnetic fields, heat, and mechanical forces, which is a central goal of condensed matter physics.

Specifically, the presence or absence of mirror symmetry can lead to a variety of unusual phases and properties. For example, the absence of mirror plane symmetry in noncentrosymmetric materials can give rise to gyrotropic order, which can lead to a nonzero Kerr rotation and a nonzero circular photo-galvanic effect [3–5]. Moreover, in SnTe, a topological crystalline insulator, the presence of mirror symmetry gives rise to conducting surface states through the existence of a nonzero mirror Chern number. This topological index guarantees an even number of Dirac cones on surfaces where mirror symmetry is retained [6–8]. In other circumstances, the existence of mirror symmetry is more controversial. One notable example is in 1/8-doped $La_{2-x}Ba_xCuO_4$, an unconventional superconductor, where coincident with the charge order transition is the appearance of an anomalous Nernst effect [9] and a nonzero polar Kerr effect [10]. The authors attributed these observations to the breaking of time-reversal symmetry and the onset of gyrotropic order, respectively. At the same time, terahertz polarimetry experiments [11] suggest that mirror symmetry may be broken well above room temperature, which would imply that the onset of gyrotropic order may result from the breaking of only inversion and roto-inversion symmetries at the charge ordering temperature.

Such controversy has led some to seek an experimental method to serve as a binary indicator of broken mirror symmetry [12]. In principle, several tools can already do this, including resonant ultrasound spectroscopy [13, 14], X-ray, neutron, and electron diffraction [15, 16], and a recently-proposed method, shear conductivity [12]. Resonant ultrasound spectroscopy and the diffraction-based techniques are more sensitive to the ionic lattice, which makes the identification of subtle electronic symmetry-breaking challenging. And while shear conductivity has the potential to be an extremely versatile tool for identifying broken point group symmetries, experimental pursuits are currently only preliminary [12]. In this study, we focus on a nonlinear optical technique, rotational-anisotropy second harmonic generation (RA-SHG), which we show is capable not only of identifying broken mirror symmetry [17] but also of resolving its sense (left- or right-handed). Furthermore, RA-SHG is sensitive to the electronic subsystem and can be used for microscopy studies, making it an ideal experimental tool for probing phase transitions where domains may arise [18, 19].

In this direction, we choose a material, $1T$-TaS_2, in which vertical mirror plane symmetry is manifestly broken across a phase transition [20, 21]. Using this material, we demonstrate in this Letter that RA-SHG, an all-optical probe sensitive to a material's point group, is an effective probe of broken mirror symmetry. We also show that the phase of the RA-SHG signal represents a physical observable that is sensitive to the planar chirality of the mirror symmetry-broken phase. Thus, RA-SHG can be used to differentiate mirror-opposite domains.

$1T$-TaS_2 is a layered material with a crystallographic structure identical to other octahedrally-coordinated transition metal dichalcogenides (Fig. 1(a)). The space group of the high temperature, undistorted phase is $P\bar{3}m1$ (no.164, point group D_{3d}) [22], and the point group of the surface normal to the (001) direction in this phase is C_{3v} [23, 24]. Upon lowering temperature, $1T$-TaS_2 undergoes a series of charge density wave (CDW)

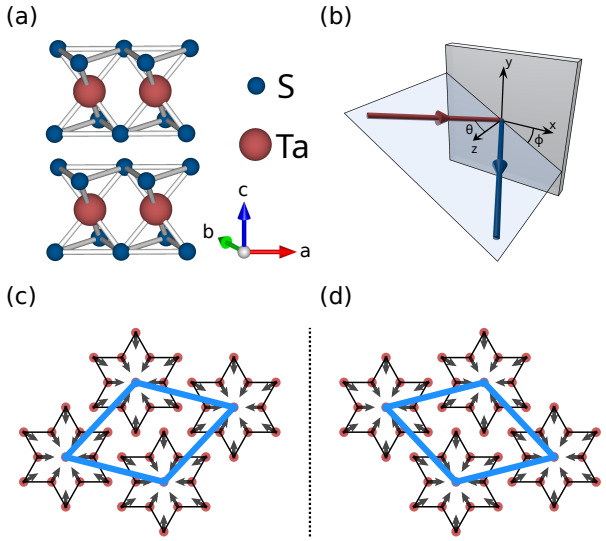

FIG. 1. (a) Structure of $1T$-TaS_2 in the undistorted phase. Ta and S atoms are depicted in red and blue, respectively. (b) Schematic of the experimental geometry. (c-d) Structure of the CDW in the NC phase. Arrows denote the movement of the Ta atoms (red) below $T_{\mathrm{IC-NC}} = 353$K from their undistorted positions. The transition at $T_{\mathrm{IC-NC}}$ spontaneously breaks mirror symmetry, so that two different CDW configurations (α and β) can form which have opposite planar chirality. The new unit cells of the two configurations are depicted in blue.

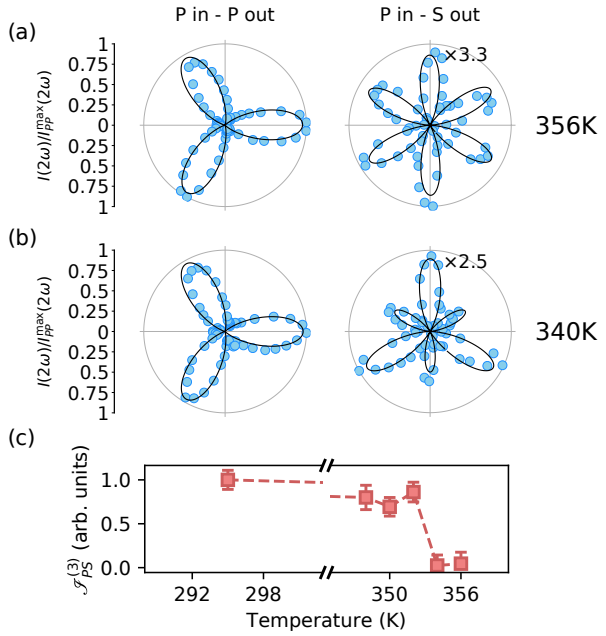

FIG. 2. (a-b) Second harmonic intensity from 1T-TaS_2 as a function of ϕ above (a) and below (b) $T_{\mathrm{IC-NC}} = 353$K. For clarity, only two polarization channels are shown; the others are reproduced in the supplement. Solid lines in (a) and (b) are best fits to the data using the surface point groups C_{3v} and C_3, respectively. Data is normalized to the maximum value of the $\mathrm{P_{in}}$-$\mathrm{P_{out}}$ signal for each temperature. (c) Temperature dependence of $\mathscr{I}_{PS}^{(3)}$ of Eq. 1.

phase transitions. At $T_{\mathrm{IC}} = 550$K, a triple-q incommensurate (IC) CDW forms which breaks translational symmetry but retains the surface point group symmetries of the undistorted phase [23, 24]. The effects of the CDW on the bulk symmetries in this phase are not yet understood. On further cooling, at $T_{\mathrm{IC-NC}} = 353$K there is a weakly first-order transition to a nearly-commensurate (NC) phase, where three vertical mirror plane symmetries are broken [22] and the surface point group becomes C_3. The NC phase has been visualized with scanning tunneling microscopy and exhibits patches of commensurate "Star of David" hexagrams that are separated by a network of discommensurations [25]. Because mirror symmetry is broken, there are two energetically equivalent CDW configurations (α and β) in the NC phase that have opposite planar chirality (Fig. 1(c)-(d)). At even lower temperatures, $T_{\mathrm{NC-C}} = 184$K, $1T$-TaS_2 undergoes a surface point group symmetry-preserving first-order transition, where the discommensurations disappear and the CDW locks into a structure commensurate with the underlying lattice [26].

Recent interest in the NC phase of $1T$-TaS_2 has arisen due to the possibility of injecting mirror-opposite domains into the structure [21], which typically do not exist in the ground state due to the absence of depolarizing fields. Zong *et al.* were able to induce these domains using a single ultrafast pulse of light, which was found to drive the material into a long-lived metastable state possessing domains of opposite planar chirality. Partly motivated by the desire to image these domains, we seek here a simple experimental method that could identify domains with opposite planar chirality.

$1T$-TaS_2 samples used in the experiment were grown using the chemical vapor transport technique, as described in Ref. [21]. In the NC phase, $1T$-TaS_2 is typically single-domain, which we have verified with electron diffraction on a sample from the same batch (see supplement). This is in agreement with previous works [20, 21, 27, 28].

In RA-SHG [29–32], a pulsed laser beam of frequency ω and amplitude $E(\omega)$ is focused onto a sample with nonzero angle of incidence θ (Fig. 1(b)). The 2ω component of the radiation emitted by the sample is subsequently measured in various combinations of incoming and outgoing polarizations (either parallel (P) or perpendicular (S) to the plane of incidence) and as a function of the angle ϕ between the plane of incidence and some crystallographic axis. In noncentrosymmetric materials, the response is dominated by the bulk electric dipole moment $P_i(2\omega) = \chi_{ijk} E_j(\omega) E_k(\omega)$ [33], where χ_{ijk} is

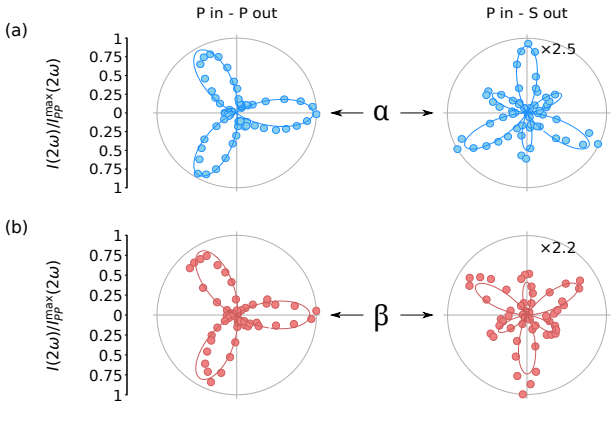

FIG. 3. Second harmonic intensity as a function of ϕ from mirror-opposite samples of $1T$-TaS_2 in the NC phase ($T = 340$K). The labels α and β refer to the two degenerate mirror-image configurations which are allowed in the NC phase. The solid line in (a) is a fit to the data using the surface point group C_3. The fit in (b) was generated by performing a mirror operation (see supplement) to the numerical susceptibility tensor obtained from (a). Data is normalized to the maximum value in the P_{in}-P_{out} polarization channel for each sample.

a material-specific susceptibility tensor which must be invariant under all symmetry operations present in the crystallographic point group. In centrosymmetric crystals such as $1T$-TaS_2, the bulk electric dipole response is forbidden by the presence of inversion symmetry [33, 34]. In this case, the dominant response often comes from the surface of the sample, which necessarily breaks inversion symmetry [35]. SHG from surfaces of materials is described by a different susceptibility tensor, χ^S_{ijk}, which is constrained by the crystal symmetries of the surface. In addition, there can be bulk contributions from higher-order processes which are allowed in the presence of inversion symmetry, such as the bulk quadrupole response $Q_{ij}(2\omega) = \chi^Q_{ijkl} E_k(\omega) E_l(\omega)$ [18, 36].

In our implementation, data was taken with the 800nm pulsed output of a regeneratively amplified Ti:Sapphire laser operating at 5kHz. The beam was scattered by a transmissive phase grating into multiple diffraction orders, and the +1-order component was steered through a polarizer and focused onto the sample to a spot diameter of $\sim 150\mu$m at a 10° angle with respect to the (001) sample normal. This experimental geometry is similar to that described in Refs. 29 and 37. The reflected light at 400nm was directed through an analyzer and into a photomultiplier tube, where the intensity was measured with a lock-in amplifier. We rotated the phase grating at $\sim$5Hz and recorded the signal as a function of ϕ (Fig. 1(b)).

To show that we are sensitive to the breaking of mirror symmetry across the IC to NC transition, we took RA-SHG data on $1T$-TaS_2 in both phases. Figs. 2(a) and 2(b) show the second harmonic response from the sample above and below $T_{IC-NC} = 353$K in two polarization channels, plotted as a function of ϕ. Despite the incommensurate nature of the charge density wave, the surface point group symmetries of the material are retained at a single point and remain well-defined. We are thus able to fit the rotational anisotropy in the IC phase using the surface point group C_{3v} (Fig. 2(a)), which is in agreement with previous reports [23, 24]. It should be noted that in order to fit the S_{in}-S_{out} polarization channel appropriately, we find that it is necessary to add an additional bulk quadrupole contribution to the signal. The consequences of this contribution will be discussed later, but at the moment they do not affect our conclusions.

Upon cooling into the NC phase, mirror symmetry is spontaneously broken and the surface point group reduces to C_3 [22]. As a result, the RA-SHG exhibits a marked lowering of symmetry (Fig. 2(b)). This lowering of symmetry can be understood by inspecting the Fourier decomposition for the rotational anisotropy,

$$I^{2\omega}_{\Gamma_{in}\Gamma_{out}}(\phi) = \sum_{n=0}^{\infty} \mathscr{I}^{(n)}_{\Gamma_{in}\Gamma_{out}} \sin\left[n\phi + \psi^{(n)}_{\Gamma_{in}\Gamma_{out}}\right], \qquad (1)$$

where $\mathscr{I}^{(n)}_{\Gamma_{in}\Gamma_{out}}$ and $\psi^{(n)}_{\Gamma_{in}\Gamma_{out}}$ refer to the amplitude and phase of the n-fold Fourier component of the SHG intensity for a particular combination of incoming (Γ_{in}) and outgoing (Γ_{out}) polarizations.

Symmetry considerations (see supplement) reveal that $\mathscr{I}^{(3)}_{PS}$ vanishes identically in the presence of mirror symmetry, leading to the six-fold symmetry in the P_{in}-S_{out} channel seen in Fig. 2(a). However, $\mathscr{I}^{(3)}_{PS}$ becomes nonzero when mirror symmetry is broken. Below T_{IC-NC}, the RA-SHG intensity subsequently exhibits a three-fold rather than a six-fold symmetric pattern, arising from a nonzero $\mathscr{I}^{(3)}_{PS}$ (Fig. 2(b)). The change of symmetry is further highlighted in the temperature dependence of $\mathscr{I}^{(3)}_{PS}$. Figure 2(c) shows that $\mathscr{I}^{(3)}_{PS}$ appears discontinuously below T_{IC-NC}, consistent with the first-order nature of the phase transition. Taken together, these observations confirm that $\mathscr{I}^{(3)}_{PS}$ is a binary indicator of broken mirror symmetry in $1T$-TaS_2.

Having established that RA-SHG is sensitive to the breaking of vertical mirror plane symmetry in $1T$-TaS_2, we now seek to demonstrate that it can differentiate between CDW configurations of opposite planar chirality in the NC phase. To do so, we generate two samples with opposite planar chirality by cleaving a single sample of $1T$-TaS_2 and perform RA-SHG on both sides of the same cleave. The act of cleaving the sample is equivalent to performing a 180° rotation about an in-plane axis, which in a single layer is equivalent to a mirror reflection (Figs. 1(c) and (d)) (see supplement).

Figure 3 shows the results of RA-SHG measurements in the P_{in}-P_{out} and P_{in}-S_{out} polarization channels as a function of ϕ, where the two mirror images are labeled α and

β. As shown in the figure, the difference between α and β configurations in RA-SHG is manifest in the phase of the signal in the P_{in}-S_{out} channel as measured with respect to the P_{in}-P_{out} channel. This phase difference explicitly indicates the sense associated with the breaking of mirror symmetry in $1T$-TaS_2. Appealing again to Eq. 1, it is possible to show (see supplement) that performing a mirror operation on the susceptibility tensor χ^S_{ijk} has the simple effect of changing the sign of $\psi^{(3)}_{PS}$. $\psi^{(3)}_{PS}$ thereby constitutes an experimental observable capable of identifying the sense associated with broken mirror symmetry in $1T$-TaS_2.

To validate the analysis contained above, we first fit the data for the α structure using the surface point group C_3 to generate a tensor χ^α_{ijk} with numerical coefficients. The fit is shown in Fig. 3(a). Then, we transform χ^α_{ijk} by a mirror reflection to generate χ^β_{ijk} (see supplement). With this transformation, we find that the rotational anisotropy simulated using χ^β_{ijk} collapses exactly onto the measured signal, as shown in Fig. 3(b).

The final observation of this work concerns the contribution from the bulk of the sample to the measured RA-SHG signal. As mentioned above, we find that in order to fit the data in all four polarization channels correctly, we need to introduce an additional contribution to the SHG signal beyond the surface electric dipole contribution. This is clear if one considers the S_{in}-S_{out} polarization channel, for which it is simple to prove (see supplement) that for purely electric dipole SHG, the three-fold SHG component $\mathscr{I}^{(3)}_{SS}$ must vanish irrespective of the point group symmetry. Fig. 4(a) and (c) show the measured RA-SHG data from $1T$-TaS_2 in the S_{in}-S_{out} polarization channel below and above T_{IC-NC}. The three-fold symmetry in these plots shows that $\mathscr{I}^{(3)}_{SS}$ is nonzero and that there must be a contribution beyond electric dipole SHG.

The next-lowest order contribution to SHG is given by the bulk electric quadrupole contribution, which is allowed in the presence of inversion symmetry [18, 36]. The electric quadrupole moment has a distinct dependence on the angle of incidence of the incoming light because the corresponding radiative source term in Maxwell's wave equation is proportional to the gradient of the quadrupole moment $\nabla_j Q_{ij} \propto \chi^Q_{ijkl} k_j E_k E_l$ [18, 36, 38]. Thus the bulk quadrupole contribution can be identified by examining the dependence of the rotational anisotropy on the incident wavevector $\boldsymbol{k}$ in the S_{in}-S_{out} polarization channel [35]. We therefore performed RA-SHG measurements on $1T$-TaS_2 in the S_{in}-S_{out} polarization channel at $\theta = 10°$ and at $\theta = 0°$. The wavevector dependence depicted in Figs. 4(a) and 4(b) establishes that the secondary contribution derives from bulk quadrupolar SHG.

Importantly, the quadrupole susceptibility tensor χ^Q_{ijkl} carries information about the bulk point group [35]. By identifying the highest-symmetry combination of surface and bulk point groups which are consistent with RA-SHG, we can therefore constrain both the surface and the bulk symmetries of the different phases in $1T$-TaS_2. In the NC phase (Fig. 4(a)-(b)), we find a nonzero value for $\mathscr{I}^{(3)}_{SS}$, which is only allowed by subgroups of the undistorted bulk point group D_{3d} which lack mirror symmetry (see supplement). This data can be fit with the bulk point group S_6 and surface point group C_3, which is consistent with diffraction measurements [24].

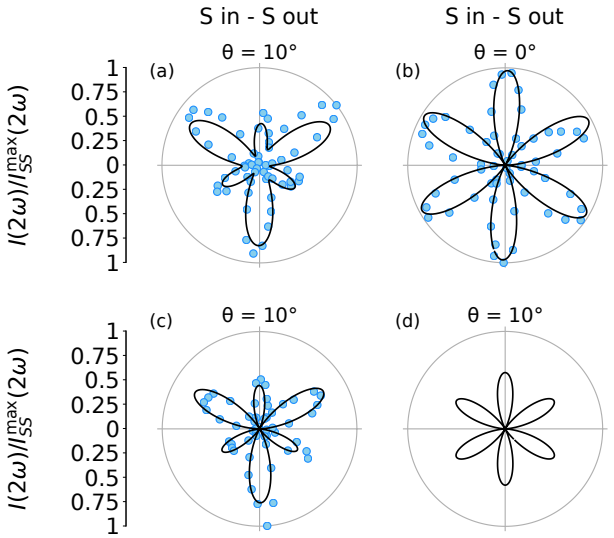

FIG. 4. Second harmonic intensity and best-fit curves as a function of ϕ in the S_{in}-S_{out} polarization channel (a) in the NC phase ($T = 295$K) at $\theta = 10°$ fit using C_3 surface dipole and S_6 bulk quadrupole contributions, (b) in the NC phase ($T = 295$K) at $\theta = 0°$ fit using C_3 surface dipole and S_6 bulk quadrupole contributions, and (c) in the IC phase ($T = 356$K) at $\theta = 10°$ fit using C_{3v} surface dipole and S_6 bulk quadrupole contributions. (d) Best fit to data in (c) using C_{3v} surface dipole and D_{3d} bulk quadrupole contributions. Data in all plots was normalized to one for clarity. Other polarization channels are depicted in the supplement.

If mirror symmetry were fully restored in the bulk of the IC phase, we would expect to be able to fit the high temperature data using a surface point group C_{3v} plus a bulk quadrupole contribution in the point group D_{3d} (Fig. 4(d)). Therefore, we would expect that $\mathscr{I}^{(3)}_{SS}$ should vanish above T_{IC-NC}. However, we find that the data in this phase (Fig. 4(c)) still maintains a positive $\mathscr{I}^{(3)}_{SS}$. This result suggests that the bulk of $1T$-TaS_2 in the IC phase breaks mirror symmetry. By fitting the data, we can subsequently identify the surface and bulk point groups as C_{3v} and S_6, respectively. Notably, we find that the surface point group C_{3v} preserves the mirror symmetry which is broken in S_6. With RA-SHG, it is not possible to deduce the full crystal structure, but we speculate that this discrepancy between surface and bulk symmetries might be attributable to the particular stack-

ing arrangement associated with the CDW above $T_{\mathrm{IC-NC}}$ (see supplement for further details). This would explain why the surface component, which is measuring the local structure at the surface of the sample [35], is consistent with the existence of mirror symmetry, whereas the bulk component, which measures the global structure of many layers, is not.

In summary, we have demonstrated here that RA-SHG can be used to identify broken mirror symmetry in crystalline materials. In addition, we have found that RA-SHG can differentiate between structural configurations related by mirror reflection, and have identified $\psi_{PS}^{(3)}$ as an indicator of the sense of planar chirality in $1T$-TaS_2. By considering the value of $\mathscr{I}_{SS}^{(3)}$, we have also shown that RA-SHG is sensitive to broken mirror symmetry in the bulk of $1T$-TaS_2, and have found evidence that the IC phase of this material breaks mirror symmetry in the bulk. In order to fully understand the origin of broken mirror symmetry in the bulk of $1T$-TaS_2, it will be necessary to perform more targeted structural studies. Nevertheless, our study opens up the possiblity for RA-SHG to detect mirror symmetry-broken phases and their domain structures in other candidate materials.

We would like to thank Adrian Po and Liang Fu for helpful discussions regarding this work. This work was supported by the Gordon and Betty Moore Foundations EPiQS Initiative Grant GBMF4540 to NG (data analysis and manuscript writing) and Grant GBMF3848 to JGC (instrumentation), Shell through the MIT Energy Initiative (experimental setup and material development) and through DARPA DSO under DRINQS program grant number D18AC00014 (sample growth and data taking). L.Y. acknowledges support by the STC Center for Integrated Quantum Materials, NSF Grant No. DMR-1231319 and by the Tsinghua Education Foundation. B.G. gratefully acknowledges the German Academic Exchange Service (DAAD) for supporting his research stay with a fellowship.

* gedik@mit.edu

[1] J. Sethna, *Statistical mechanics: entropy, order parameters, and complexity* (Oxford University Press, 2006).
[2] D. Thouless, *Topological quantum numbers in nonrelativistic physics* (World Scientific, 1998).
[3] P. Hosur, A. Kapitulnik, S. A. Kivelson, J. Orenstein, and S. Raghu, Phys. Rev. B **87**, 115116 (2013).
[4] P. Hosur, A. Kapitulnik, S. A. Kivelson, J. Orenstein, S. Raghu, W. Cho, and A. Fried, Phys. Rev. B **91**, 039908 (2015).
[5] V. Belinicher and B. Sturman, Soviet Physics Uspekhi **23**, 199 (1980).
[6] J. C. Y. Teo, L. Fu, and C. L. Kane, Phys. Rev. B **78**, 045426 (2008).
[7] T. H. Hsieh, H. Lin, J. Liu, W. Duan, A. Bansil, and L. Fu, Nature Communications **3** (2012), 10.1038/ncomms1969.
[8] L. Fu, Physical Review Letters **106** (2011), 10.1103/PhysRevLett.106.106802.
[9] L. Li, N. Alidoust, J. M. Tranquada, G. D. Gu, and N. P. Ong, Phys. Rev. Lett. **107**, 277001 (2011).
[10] H. Karapetyan, J. Xia, M. Hücker, G. D. Gu, J. M. Tranquada, M. M. Fejer, and A. Kapitulnik, Phys. Rev. Lett. **112**, 047003 (2014).
[11] Y. Lubashevsky, L. Pan, T. Kirzhner, G. Koren, and N. P. Armitage, Phys. Rev. Lett. **112**, 147001 (2014).
[12] P. Hlobil, A. V. Maharaj, P. Hosur, M. C. Shapiro, I. R. Fisher, and S. Raghu, Physical Review B **92** (2015), 10.1103/PhysRevB.92.035148.
[13] R. G. Leisure and F. Willis, Journal of Physics: Condensed Matter **9**, 6001 (1997).
[14] A. Migliori, J. Sarrao, W. M. Visscher, T. Bell, M. Lei, Z. Fisk, and R. G. Leisure, Physica B: Condensed Matter **183**, 1 (1993).
[15] G. E. Bacon, *X-ray and Neutron Diffraction* (Elsevier, 1966).
[16] D. L. Dorset, *Structural electron crystallography* (Springer Science & Business Media, 2013).
[17] T. F. Heinz, M. M. T. Loy, and W. A. Thompson, Phys. Rev. Lett. **54**, 63 (1985).
[18] D. H. Torchinsky and D. Hsieh, in *Magnetic Characterization Techniques for Nanomaterials*, edited by C. S. Kumar (Springer Berlin Heidelberg, Berlin, Heidelberg, 2017) pp. 1–40.
[19] J. W. Harter, Z. Y. Zhao, J.-Q. Yan, D. G. Mandrus, and D. Hsieh, Science **356**, 295 (2017).
[20] J. Wilson, F. Di Salvo, and S. Mahajan, Advances in Physics **24**, 117 (1975).
[21] A. Zong, X. Shen, A. Kogar, L. Ye, C. Marks, D. Chowdhury, T. Rohwer, B. Freelon, S. Weathersby, R. Li, J. Yang, J. Checkelsky, X. Wang, and N. Gedik, Science Advances **4** (2018), 10.1126/sciadv.aau5501.
[22] A. Spijkerman, J. L. de Boer, A. Meetsma, G. A. Wiegers, and S. van Smaalen, Physical Review B **56**, 13757 (1997).
[23] C. B. Scruby, P. M. Williams, and G. S. Parry, Philosophical Magazine **31**, 255 (1975).
[24] K. Fung, J. Steeds, and J. Eades, Physica B+C **99**, 47 (1980).
[25] X. L. Wu and C. M. Lieber, Science **243**, 1703 (1989).
[26] T. Ishiguro and H. Sato, Physical Review B **52**, 759 (1995).
[27] M. Bovet, D. Popovi, F. Clerc, C. Koitzsch, U. Probst, E. Bucher, H. Berger, D. Naumovi, and P. Aebi, Physical Review B **69** (2004), 10.1103/PhysRevB.69.125117.
[28] K. N. H. Shiba, in *Structural Phase Transitions in Layered Transition Metal Compounds*, edited by K. Motizuki (D. Reidel Publishing Company, 1986) pp. 175–266.
[29] J. W. Harter, L. Niu, A. J. Woss, and D. Hsieh, Optics Letters **40**, 4671 (2015).
[30] B. Lu, J. D. Tran, and D. H. Torchinsky, Review of Scientific Instruments **90**, 053102 (2019), https://doi.org/10.1063/1.5080965.
[31] D. H. Torchinsky, H. Chu, L. Zhao, N. B. Perkins, Y. Sizyuk, T. Qi, G. Cao, and D. Hsieh, Physical Review Letters **114** (2015), 10.1103/PhysRevLett.114.096404.
[32] B. Lu and D. H. Torchinsky, Opt. Express **26**, 33192 (2018).
[33] R. Boyd, *Nonlinear Optics*, 3rd ed. (Academic Press, 2008).

[34] R. C. Powell, *Symmetry, Group Theory, and the Physical Properties of Crystals*, 1st ed., Lecture Notes in Physics, Vol. 824 (Springer-Verlag, New York, 2010).
[35] N. Bloembergen, R. K. Chang, S. S. Jha, and C. H. Lee, Physical Review **174**, 813 (1968).
[36] Y. Shen, *The Principles of Nonlinear Optics*, Pure & Applied Optics Series: 1-349 (Wiley, 1984).
[37] D. H. Torchinsky, H. Chu, T. Qi, G. Cao, and D. Hsieh, Review of Scientific Instruments **85**, 083102 (2014).
[38] J. D. Jackson, *Classical Electrodynamics*, 3rd ed. (Wiley, 1998).

Supplementary Material for Second Harmonic Generation as a Probe of Broken Mirror Symmetry in a Charge Density Wave Transition

Bryan T. Fichera,[1] Anshul Kogar,[1] Linda Ye,[1] Bilal Göcke,[1,2] Alfred Zong,[1] Joseph G. Checkelsky,[1] and Nuh Gedik[1,*]

[1] *Department of Physics, Massachusetts Institute of Technology, Cambridge, Massachusetts 02139, USA*
[2] *Technical Chemistry I and Center for Nanointegration Duisburg-Essen (CENIDE), University of Duisburg-Essen, 45141 Essen, Germany*

(Dated: October 8, 2019)

S1. PROBING BROKEN MIRROR SYMMETRY WITH RA-SHG

A. Complete RA-SHG data

In the first section of the main text, we discuss how RA-SHG is sensitive to the breaking of mirror symmetry in 1T-TaS_2. In Figs. 2(a) and 2(b) of the main text, we display RA-SHG data in two polarization channels: P_{in}-P_{out} and P_{in}-S_{out}. For completeness, the other polarization channels are reproduced in Fig. S1. Importantly, the fits in the figure only include a surface electric dipole contribution (see main text). The inability to fit the S_{in}-S_{out} polarization channel with a pure electric dipole contribution suggested to us that a second contribution was necessary in the form of a bulk electric quadrupole term. This is discussed in the main text as well as in section S4.

B. $\mathscr{I}_{PS}^{(3)}$ as an indicator of broken mirror symmetry

Given any crystallographic point group, it is always possible to compute the form of the susceptibility tensor χ_{ijk}^S. In C_3, the susceptibility tensor is given by[1]

$$\chi_{ijk}^S = \left(\begin{array}{ccc} \chi_{xxx} & -\chi_{yyy} & \chi_{yyz} \\ -\chi_{yyy} & -\chi_{xxx} & -\chi_{yxz} \\ \chi_{yyz} & -\chi_{yxz} & 0 \\ \hline -\chi_{yyy} & -\chi_{xxx} & \chi_{yxz} \\ -\chi_{xxx} & \chi_{yyy} & \chi_{yyz} \\ \chi_{yxz} & \chi_{yyz} & 0 \\ \hline \chi_{zyy} & 0 & 0 \\ 0 & \chi_{zyy} & 0 \\ 0 & 0 & \chi_{zzz} \end{array}\right)_{ijk}. \tag{S1}$$

In the point group C_{3v}, the susceptibility tensor is constrained by symmetry so as to take a form similar to equation S1, but with various elements removed or equated:

$$\chi_{ijk}^S = \left(\begin{array}{ccc} 0 & -\chi_{yyy} & \chi_{yyz} \\ -\chi_{yyy} & 0 & 0 \\ \chi_{yyz} & 0 & 0 \\ \hline -\chi_{yyy} & 0 & 0 \\ 0 & \chi_{yyy} & \chi_{yyz} \\ 0 & \chi_{yyz} & 0 \\ \hline \chi_{zyy} & 0 & 0 \\ 0 & \chi_{zyy} & 0 \\ 0 & 0 & \chi_{zzz} \end{array}\right)_{ijk} \tag{S2}$$

From the susceptibility tensor χ_{ijk}^S, one can then compute the RA-SHG intensity

$$I_{PS}^{2\omega}(\phi) = \left| R(\phi)_{yl} R(\phi)_{jm} R(\phi)_{kn} \chi_{lmn}^S E_j(\omega) E_k(\omega) \right|^2, \tag{S3}$$

where

$$R(\phi) = \begin{pmatrix} \cos\phi & -\sin\phi & 0 \\ \sin\phi & \cos\phi & 0 \\ 0 & 0 & 1 \end{pmatrix}, \tag{S4}$$

and $\boldsymbol{E}(\omega) = (-\cos\theta, 0, \sin\theta)^T$. Here we use that the sample normal is along (001).

It is easy to then compute the Fourier transform of $I_{PS}^{2\omega}(\phi)$ defined by Eq. 1. The parameters $I_{PS}^{(n)}$ and $\psi_{PS}^{(n)}$ are then simple functions of the susceptibility tensor elements. In the low temperature phase, where mirror symmetry is broken, we find

$$\mathscr{I}_{PS}^{(3)}(\chi_{ijk}^S) = 4\sqrt{a_1^2 + a_2^2} \tag{S5}$$

and

$$\psi_{PS}^{(3)}(\chi_{ijk}^S) = \text{atan2}\left(a_1, a_2\right) \tag{S6}$$

where

$$a_1 = -\chi_{yyy} \cdot \chi_{yxz} \sin\theta \cos^3\theta, \tag{S7}$$

$$a_2 = \chi_{xxx} \cdot \chi_{yxz} \sin\theta \cos^3\theta, \tag{S8}$$

θ is the angle of incidence, and

$$\text{atan2}\left(y, x\right) \equiv \begin{cases} \arctan\left(\frac{y}{x}\right) & x > 0 \\ \arctan\left(\frac{y}{x}\right) + \pi & y > 0, x < 0 \\ \arctan\left(\frac{y}{x}\right) - \pi & y < 0, x < 0 \\ +\frac{\pi}{2} & y > 0, x = 0 \\ -\frac{\pi}{2} & y < 0, x = 0 \\ \text{undefined} & x = y = 0 \end{cases}. \tag{S9}$$

By comparing equations S2 and S1, we find that

$$a_1 = a_2 = 0 \tag{S10}$$

in the high temperature phase, so that $\mathscr{I}_{PS}^{(3)}(\chi_{ijk}) = 0$.

Note that Eq. S5 highlights an important aspect of our experiment, which is that the binary indicator, $\mathscr{I}_{PS}^{(3)}$, requires a nonzero angle of incidence to be observed, i.e.

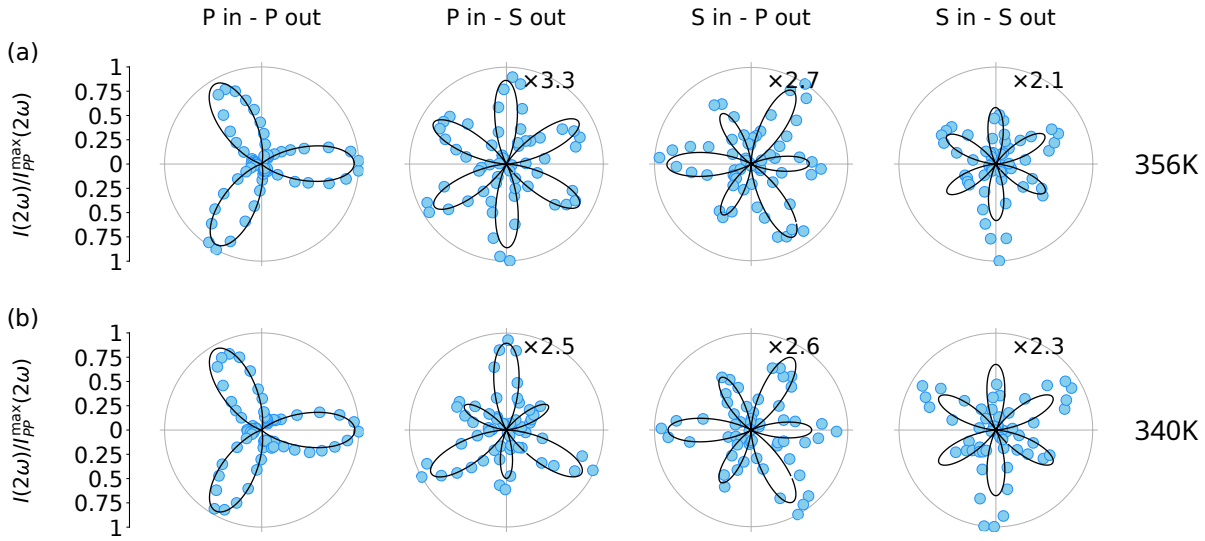

FIG. S1. RA-SHG intensity as a function of ϕ above (a) and below (b) $T_{IC-NC} = 353K$. Solid lines are are best fits to the data using electric dipole SHG in the surface point groups C_{3v} and C_3, respectively. Data is normalized to the maximum value of the P_{in}-P_{out} signal for each temperature.

RA-SHG at normal incidence on the (001) surface of 1T-TaS_2 is not capable of resolving broken vertical mirror plane symmetry. This can be understood by noting that $\mathscr{I}_{PS}^{(3)}$ is nonzero only when the tensor element χ_{yxz}^S is nonzero. However, for such a term to be observable in the experiment, there needs to be an out-of-plane component to the incoming electric fields, which in turn requires a nonzero angle of incidence. Moreover, in a system with three-fold symmetry like 1T-TaS_2, the aforementioned tensor element can only be nonzero in a system where mirror symmetry is absent. To see that this is true, consider the term $P_y(2\omega) = \chi_{yxz}^S E_x(\omega)E_z(\omega)$. Under an $x \to -x$ mirror operation, we require that $P_y \to P_y$, $E_x \to -E_x$, $E_z \to E_z$, and $\chi_{yxz}^S \to \widetilde{\chi}_{yxz}^S$. However, if this operation is a symmetry of the crystal then we have $\widetilde{\chi}_{yxz}^S = \chi_{yxz}^S$, so that $P_y = -P_y$. This implies that $\chi_{yxz}^S = 0$. Therefore both a nonzero angle of incidence and broken mirror symmetry are required for a nonzero $\mathscr{I}_{PS}^{(3)}$ in the geometry of our experiment.

S2. IMPORTANCE OF THE P_{in}-S_{out} CHANNEL AND GENERALIZATION TO OTHER MIRROR-SYMMETRY-BREAKING TRANSITIONS

In this section we explain physically why the P_{in}-S_{out} polarization channel is the most sensitive to mirror symmetry breaking in 1T-TaS_2, and generalize the analysis in the present work to other phase transitions in which mirror symmetry is broken. Consider the experimental geometry depicted in Fig. S2(a). A P-polarized electric field $\boldsymbol{E}_{in}$ is incident in a plane parallel to the z axis on a sample with vertical mirror symmetry about the xz plane (indicated by the sides A and B of the sample being the same color). The geometry is such that the plane of incidence makes an angle ϕ with the reflection plane. Let $\boldsymbol{P}_\perp(\phi)$ be the S-polarized component of the polarization resulting from second harmonic generation by the interaction of the sample with $\boldsymbol{E}_{in}$.

Now consider applying the mirror operation both to $\boldsymbol{E}_{in}$ and to the sample (Fig. S2(b)). Then the resulting S-polarized component of the polarization (in the frame of the plane of incidence) will be $-\boldsymbol{P}_\perp(\phi)$. However, since the sides A and B in Fig. S2(b) are the same, by symmetry the problem is equivalent to Fig. S2(a) but with ϕ replaced by $-\phi$. Thus $\boldsymbol{P}_\perp(-\phi) = -\boldsymbol{P}_\perp(\phi)$, implying that $\boldsymbol{P}_\perp(0) = \boldsymbol{P}_\perp(\pi) = 0$. This along with threefold rotational symmetry is sufficient to prove that the RA-SHG pattern from IC-phase 1T-TaS_2 in the P_{in}-S_{out} polarization channel is purely sixfold-symmetric. However, in the case where mirror symmetry is broken (Figs. S2(c-d)) the above argument no longer holds and the constraint $\boldsymbol{P}_\perp(-\phi) = -\boldsymbol{P}_\perp(\phi)$ is relaxed. Therefore in 1T-TaS_2, $\mathscr{I}_{\mathrm{PS}}^{(3)}$ is allowed in the NC phase but not in the IC phase.

In contrast to the S-polarized output ($\boldsymbol{P}_\perp(\phi)$), the P-polarized output ($\boldsymbol{P}_\parallel(\phi)$) does not change sign (as defined in the frame of the plane of incidence) under mirror reflection. Therefore the constraint for P-polarized output is that $\boldsymbol{P}_\parallel(\phi) = \boldsymbol{P}_\parallel(-\phi)$. Importantly, this constraint does not forbid fourier components like $\mathscr{I}_{\mathrm{PP}}^{(3)}$ and $\mathscr{I}_{\mathrm{SP}}^{(3)}$, even when mirror symmetry is present.

Finally, while the S_{in}-S_{out} channel is subject to the constraint $\boldsymbol{P}_\perp(-\phi) = -\boldsymbol{P}_\perp(\phi)$, it can also be shown (see section S4 B) that in the electric dipole regime, S_{in}-S_{out} is twofold-symmetric regardless of the crystallographic

Initial group	Final group	Indicator(s)
T_d	T	None
T_d	D_{2d}	None
T_d	C_{3v}	None
C_{6v}	C_{3v}	$\mathscr{I}_{PP}^{(3)}$, $\mathscr{I}_{PP}^{(6)}$, $\mathscr{I}_{PS}^{(0)}$, $\mathscr{I}_{PS}^{(6)}$, $\mathscr{I}_{SP}^{(3)}$, $\mathscr{I}_{SP}^{(6)}$, $\mathscr{I}_{SS}^{(0)}$, $\mathscr{I}_{SS}^{(6)}$
C_{6v}	C_{2v}	$\mathscr{I}_{PP}^{(2)}$, $\mathscr{I}_{PP}^{(4)}$, $\mathscr{I}_{PS}^{(0)}$, $\mathscr{I}_{PS}^{(4)}$, $\mathscr{I}_{SP}^{(2)}$, $\mathscr{I}_{SP}^{(4)}$
C_{6v}	C_6	$\mathscr{I}_{PS}^{(0)}$
C_{4v}	C_{2v}	$\mathscr{I}_{PP}^{(2)}$, $\mathscr{I}_{PP}^{(4)}$, $\mathscr{I}_{PS}^{(0)}$, $\mathscr{I}_{PS}^{(4)}$, $\mathscr{I}_{SP}^{(2)}$, $\mathscr{I}_{SP}^{(4)}$
C_{4v}	C_4	$\mathscr{I}_{PS}^{(0)}$
D_{3h}	C_{3h}	$\psi_{PP}^{(6)*}$, $\psi_{PS}^{(6)*}$, $\psi_{SP}^{(6)*}$, $\psi_{SS}^{(6)*}$
D_{3h}	C_{2v}	None
D_{3h}	D_3	$\mathscr{I}_{PS}^{(3)}$
C_{3h}	C_3	$\psi_{PP}^{(1)*}$, $\psi_{PP}^{(2)*}$, $\psi_{PP}^{(3)*}$, $\psi_{PP}^{(4)*}$, $\psi_{PP}^{(5)*}$, $\psi_{PP}^{(6)*}$, $\psi_{PS}^{(1)*}$, $\psi_{PS}^{(2)*}$, $\psi_{PS}^{(3)*}$, $\psi_{PS}^{(4)*}$, $\psi_{PS}^{(5)*}$, $\psi_{PS}^{(6)*}$, $\psi_{SP}^{(1)*}$, $\psi_{SP}^{(2)*}$, $\psi_{SP}^{(3)*}$, $\psi_{SP}^{(4)*}$, $\psi_{SP}^{(5)*}$, $\psi_{SP}^{(6)*}$, $\psi_{SS}^{(2)*}$, $\psi_{SS}^{(4)*}$, $\psi_{SS}^{(6)*}$
C_{3v}	C_3	$\psi_{PP}^{(3)}$, $\psi_{PP}^{(6)*}$, $\mathscr{I}_{PS}^{(3)}$, $\psi_{PS}^{(6)*}$, $\psi_{SP}^{(3)}$, $\psi_{SP}^{(6)*}$, $\psi_{SS}^{(6)*}$
C_{3v}	C_{1h}	$\mathscr{I}_{PP}^{(1)}$, $\mathscr{I}_{PP}^{(2)}$, $\mathscr{I}_{PP}^{(4)}$, $\mathscr{I}_{PP}^{(5)}$, $\mathscr{I}_{PS}^{(1)}$, $\mathscr{I}_{PS}^{(2)}$, $\mathscr{I}_{PS}^{(3)}$, $\mathscr{I}_{PS}^{(4)}$, $\mathscr{I}_{PS}^{(5)}$, $\mathscr{I}_{SP}^{(1)}$, $\mathscr{I}_{SP}^{(2)}$, $\mathscr{I}_{SP}^{(4)}$, $\mathscr{I}_{SP}^{(5)}$, $\mathscr{I}_{SS}^{(2)}$, $\mathscr{I}_{SS}^{(4)}$
D_{2d}	S_4	$\psi_{PP}^{(4)*}$, $\psi_{PS}^{(4)*}$, $\psi_{SP}^{(4)*}$
D_{2d}	D_2	$\mathscr{I}_{PS}^{(2)}$
C_{2v}	C_2	$\psi_{PP}^{(2)*}$, $\psi_{PP}^{(4)*}$, $\mathscr{I}_{PS}^{(2)}$, $\psi_{PS}^{(4)*}$, $\psi_{SP}^{(2)*}$, $\psi_{SP}^{(4)*}$
C_{2v}	C_{1h}	$\mathscr{I}_{PP}^{(1)}$, $\mathscr{I}_{PP}^{(3)}$, $\mathscr{I}_{PP}^{(5)}$, $\mathscr{I}_{PP}^{(6)}$, $\mathscr{I}_{PS}^{(1)}$, $\mathscr{I}_{PS}^{(2)}$, $\mathscr{I}_{PS}^{(3)}$, $\mathscr{I}_{PS}^{(5)}$, $\mathscr{I}_{PS}^{(6)}$, $\mathscr{I}_{SP}^{(1)}$, $\mathscr{I}_{SP}^{(3)}$, $\mathscr{I}_{SP}^{(5)}$, $\mathscr{I}_{SP}^{(6)}$, $\mathscr{I}_{SS}^{(0)}$, $\mathscr{I}_{SS}^{(2)}$, $\mathscr{I}_{SS}^{(4)}$, $\mathscr{I}_{SS}^{(6)}$

* Measured from $\pi/2$

TABLE S1. Indicators of broken mirror symmetry in mirror-symmetry-breaking transitions between noncentrosymmetric point groups. Values in the rightmost column (defined in the main text) are zero in the initial group and nonzero in the final group. In all cases, the analysis was done in a geometry such that the sample normal is parallel to the broken mirror plane (i.e. the mirror plane is vertical).

point group. Therefore the P_{in}-S_{out} polarization channel is especially sensitive to the breaking of vertical mirror plane symmetry in the geometry depicted in Fig. S2.

While the argument above is effective in the case of a C_{3v} to C_3 transition (as in $1T$-TaS_2), the presence or absence of other symmetries in different point groups may call for symmetry arguments which differ from those above. Therefore, to generalize this work we provide in Table S1 a list of mirror-symmetry-breaking transitions between noncentrosymmetric point groups and identify corresponding binary indicators (like $\mathscr{I}_{\text{PS}}^{(3)}$ in $1T$-TaS_2) which can be used to identify broken mirror symmetry (note that while RA-SHG is only nonzero in noncentrosymmetric point groups, it can still be used in centrosymmetric materials because crystal surfaces necessarily break inversion symmetry).

In most of the transtions in Table S1, $\mathscr{I}_{PS}^{(n)}$ can be used as an indicator of broken mirror symmetry for some n. However, for others the RA-SHG pattern rotates rather than (or in addition to) changing symmetry, which is indicated by a change in the phase of certain Fourier components. Additionally, it should be observed that for a minority of the transitions in Table S1, RA-SHG is not sensitive to the breaking of mirror symmetry (e.g. in the transition from T_d to T, two point groups for which the susceptibility tensor is equivalent).

S3. PROBING THE SENSE OF PLANAR CHIRALITY WITH RA-SHG

A. Complete RA-SHG data

As in section S1 A, for completeness we reproduce in Fig. S3 the RA-SHG data in the α and β CDW configurations, including the two polarization channels which were truncated from Fig. 3 in the main text. The poor fit in the S_{in}-S_{out} polarization channel again indicated to

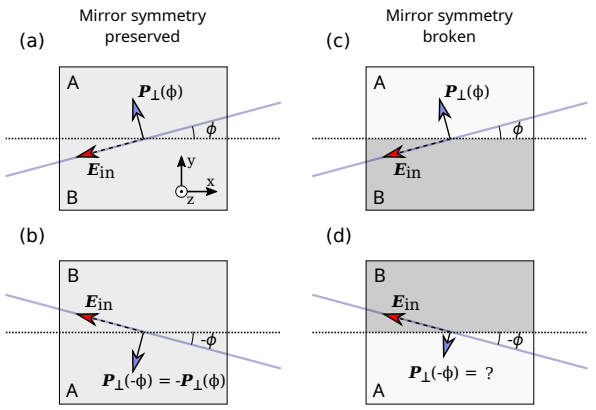

FIG. S2. (a) Geometry referenced in showing that the P_{in}-S_{out} geometry is sensitive to the breaking of vertical mirror symmetry. $\boldsymbol{E}_{in}$ is the input electric field and $\boldsymbol{P}_\perp$ is the S-polarized component of the polarization. The arrow identifying the direction of $\boldsymbol{E}_{in}$ is dashed to indicate that there is a component in the z-direction (out of the page). The solid blue and dotted black lines represent the plane of incidence and the mirror symmetry plane, respectively, which are in the z-direction and make an angle ϕ with each other. The two halves (A and B) of the sample are the same color to indicate that mirror symmetry is present in this sample. (b) Mirror image of (a), showing that $\boldsymbol{P}_\perp$ flips sign (when measured in the frame of the plane of incidence) under mirror reflection. (c) Same geometry as (a) with broken mirror symmetry, represented by the difference in color between sides A and B. (d) Mirror image of (c).

us that there was an additional bulk quadrupole contribution to the signal.

B. Electron diffraction confirming the sample is single domain

To confirm that $1T$-TaS_2 is single-domain in the NC phase, we performed electron diffraction on a sample from the same batch as the one used for the RA-SHG measurements. The absence of CDW sister peaks in Fig. S4 demonstrates that the sample is single-domain, in agreement with previous reports[2–5]. We note that recent studies have demonstrated that it is possible to inject mirror domains into an otherwise uniform sample of $1T$-TaS_2 using intense pulses of light[2]. To control for this effect, we used incident fluences which are well below the threshold fluence 5mJ/cm^2 reported in Ref. 2.

C. Fitting RA-SHG data in the α and β configurations

To fit the data in Fig. 3 of the main text, we performed the following procedure. First, we used the 6 independent elements in the C_3 susceptibility tensor given by equation S1 as fitting parameters to fit the data on the α sample (Fig. S3(a)) to

$$|P_i(\phi)|^2 = |R(\phi)_{il}R(\phi)_{jm}R(\phi)_{kn}\chi^S_{lmn}E_j(\omega)E_k(\omega)|^2. \tag{S11}$$

The fit was constrained in such a way as to forbid large changes in the susceptibility elements χ_{yyy}, χ_{yyz}, χ_{zyy}, and χ_{zzz} that exist in both phases (see Eqs. S1 and S2) from above to below $T_{\mathrm{IC-NC}} = 353K$. This gave us a set of 6 numbers $\{\chi^\alpha_{ijk}\}$, from which we can form the tensor χ^α_{ijk}. The cleaving operation can be represented by the operator $\mathcal{C} = A\Gamma(\gamma)R_x$, where R_x is the operator which rotates the sample 180° about the x-axis,

$$R_x = \begin{pmatrix} 1 & 0 & 0 \\ 0 & -1 & 0 \\ 0 & 0 & -1 \end{pmatrix}, \tag{S12}$$

$\Gamma(\gamma)$ is the operator which rotates the sample about the z-axis by an arbitrary angle γ,

$$\Gamma(\gamma) = \begin{pmatrix} \cos\gamma & -\sin\gamma & 0 \\ \sin\gamma & \cos\gamma & 0 \\ 0 & 0 & 1 \end{pmatrix}. \tag{S13}$$

and A is a positive overall constant which represents minor, day-to-day fluctuations in experimental conditions. If we were able to cleave the sample exactly along the high-symmetry axis, then γ would be 0° and $\Gamma(\gamma)$ would be identity. Also note that the fact that the determinant of $\mathcal{C}$ in the (x, y) subspace is -1 is equivalent to the statement that $\mathcal{C}$ switches the planar chirality of the sample.

To simulate the effect of cleaving the sample, we therefore applied $\mathcal{C}$ to χ^α_{ijk} to form $\chi^\beta_{ijk}(\{\chi^\alpha_{ijk}\}, \gamma, A)$. Formally, this amounts to computing

$$\chi^\beta_{ijk}(\{\chi^\alpha_{ijk}\}, \gamma, A) = \mathcal{C}_{il}(\gamma, A)\mathcal{C}_{jm}(\gamma, A)\mathcal{C}_{kn}(\gamma, A)\chi^\alpha_{lmn}. \tag{S14}$$

Now, $\chi^\beta_{ijk}(\{\chi^\alpha_{ijk}\}, \gamma, A)$ is a function of only two free parameters (γ and A). We find that with the proper choice of γ and A, the signal computed by equation S3 collapses onto the data in Fig. S3(b). This procedure also reproduces the change of the phase of the RA-SHG in the P_{in}-S_{out} channel.

D. $\psi^{(3)}_{PS}$ as an indicator for the sense of planar chirality

In the main text we argue that $\psi^{(3)}_{PS}$ can be used as an indicator for the sense of the planar chirality in $1T$-TaS_2. To show that this is true, we again appeal to the analysis in section S1 B.

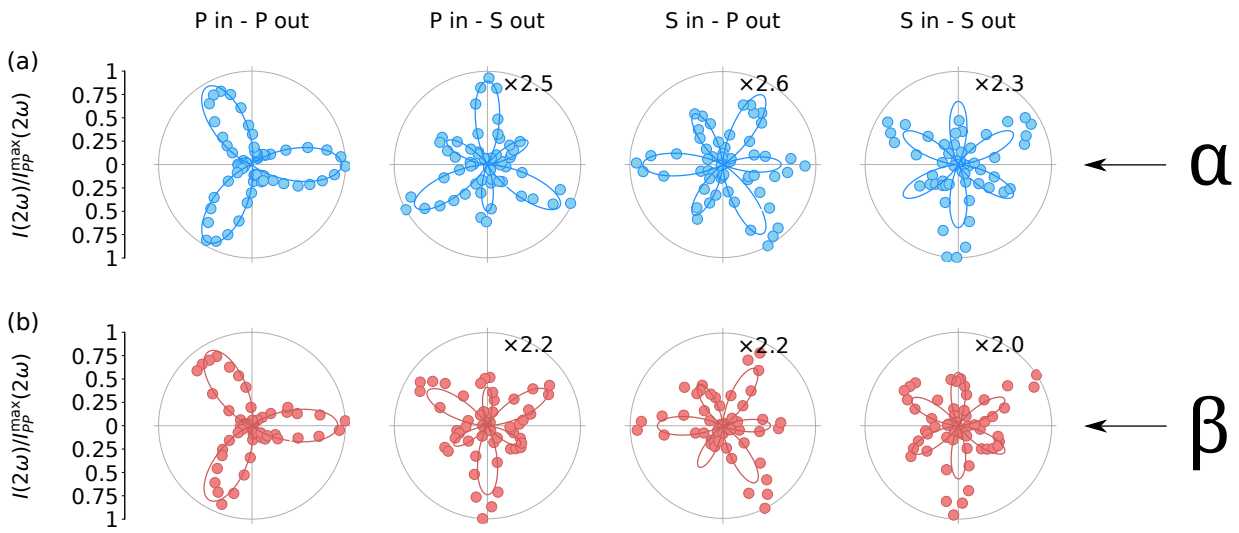

FIG. S3. Second harmonic intensity as a function of ϕ from two samples of $1T$-TaS_2 in the NC phase ($T = 340K$). The labels α and β refer to the two degenerate mirror-image configurations which can exist in the NC phase. The solid line in (a) is a fit to the data using the surface point group C_3. The fit in (b) was generated by performing a mirror operation (see section S3 C) to the numerical susceptibility tensor obtained from (a). Data is normalized to the maximum value in the P_{in}-P_{out} polarization channel for each sample.

We seek to prove that cleaving the sample (i.e. applying $\mathcal{C}$ to χ^{α}_{ijk}) has the effect of flipping the sign of $\psi^{(3)}_{PS}$. Without loss of generality, we can restrict our analysis to the case where $\gamma = 0$ and $A = 1$, so that

$$\mathcal{C} = R_x = \begin{pmatrix} 1 & 0 & 0 \\ 0 & -1 & 0 \\ 0 & 0 & -1 \end{pmatrix} \tag{S15}$$

in the 3D polar vector representation. We apply $\mathcal{C}$ to χ^{α}_{ijk} in the same way as in equation S14. By inspection, we find that $\mathcal{C}$ has the effect of changing the sign of each element with an odd number of y and z indices. This transformation negates a_1, but not a_2. Therefore $\mathcal{C}$ flips the sign of $\psi^{(3)}_{PS} = \text{atan2}\,(a_1, a_2)$.

S4. BULK BROKEN MIRROR SYMMETRY IN $1T$-TAS_2

A. Complete RA-SHG data at $T = 295K$

As in section S3 A, for completeness we reproduce in Fig. S5 the RA-SHG data at $T = 295K$ (NC phase) which is used in Fig. 4 to argue that there is a nonzero bulk electric quadrupole component to the measured signal. Furthermore, we reproduce in Fig. S6 the RA-SHG data at $T = 356K$ (IC phase), to show that we can fit all four polarization combinations using the surface point group C_{3v} as well as a bulk point group S_6 (see below). The S_{in}-S_{out} channel of Fig. S6 is shown in Fig. 4 of the main text.

B. Symmetry analysis of RA-SHG data

In the last section of the main text, we claim that the nonzero value of $\mathscr{I}^{(3)}_{SS}$ measured in Fig. 4(c) suggests the presence of broken mirror symmetry in the bulk of $1T$-TaS_2 in the IC phase, which has not been identified explicitly by other techniques. The central argument revolved around a number of symmetry constraints on $\mathscr{I}^{(3)}_{SS}$, which could be used to restrict the space of possible point groups. In this section, we provide derivations for these constraints.

To begin, we noted in the main text that the nonzero value of $\mathscr{I}^{(3)}_{SS}$ in Figs. 4(a) and 4(c) immediately suggests the presence of an SHG contribution beyond the typical surface electric dipole contribution expected from $1T$-TaS_2. This is because, for purely electric dipole SHG, the rotational anisotropy $I^{2\omega}_{SS}(\phi)$ always has at least twofold symmetry in ϕ. To see that this is true, consider the effect of taking $\phi \to \phi + \pi$ in an S-polarized input geometry. In the frame where the sample is stationary, this simply changes the sign of the input field. Since the polarization is proportional to the square of the input field ($P_i(2\omega) = \chi_{ijk}E_jE_k$), then it will be symmetric under $\phi \to \phi + \pi$, as will be its projection out of the plane of incidence (note, however, that because the component of $\boldsymbol{P}(2\omega)$ parallel to the direction of propogation is not visible in the experiment, the same cannot be said

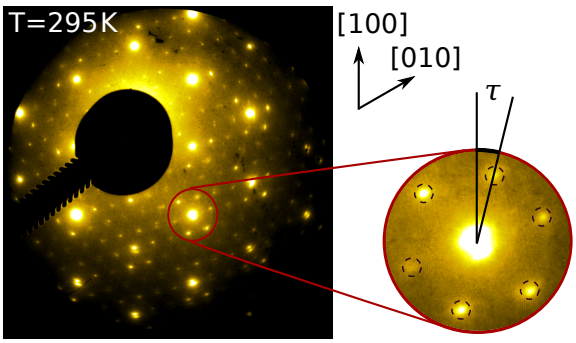

FIG. S4. Electron diffraction data from a sample of $1T$-TaS_2 in the NC phase of the same batch as the one used in RA-SHG measurements. Surrounding each Bragg reflection can be seen six CDW peaks, which are rotated about $\tau = 13°$ from the high-symmetry axes. The sign of the rotation angle τ indicates whether the CDW configuration is α or β. The lack of additional CDW peaks $-13°$ from the high-symmetry axes indicates that the sample is single-domain.

for the P-polarized output). Therefore, if the measured RA-SHG in the S_{in}-S_{out} channel lacks twofold symmetry, then there is a contribution to the rotational anisotropy which exists beyond the electric dipole.

In Fig. 4 of the main text, we see that $1T$-TaS_2 shows a clear lack of twofold symmetry in the S_{in}-S_{out} polarization channel. Having thus established that there is an additional contribution to the measured RA-SHG signal in $1T$-TaS_2, we then argue in the main text that the bulk quadrupole contribution $Q_{ij}(2\omega) = \chi^Q_{ijkl} E_k(\omega) E_l(\omega)$, which is allowed in centrosymmetric materials, is the next leading order term allowed in $1T$-TaS_2.

To check that this contribution is indeed present in $1T$-TaS_2, we note in the main text that the electric field radiated by an oscillating quadrupole moment is actually proportional to the divergence of $Q_{ij}(2\omega)$

$$\nabla_j Q_{ij}(2\omega) \propto 2i\chi^Q_{ijkl} k_j E_k(\omega) E_l(\omega), \tag{S16}$$

where $\boldsymbol{k}$ is the wavevector of the incident radiation. Importantly, despite the independence of the incident field $\boldsymbol{E} = (0,1,0)^T$ and outgoing polarization $\boldsymbol{P}(2\omega) = (0, P_y(2\omega), 0)^T$ on the angle of incidence θ in the S_{in}-S_{out} polarization channel, Eq. S16 indicates that in the presence of electric quadrupole SHG, the measured rotational anisotropy will depend on θ. This is in contrast to purely electric dipole SHG (Eq. S3), for which the signal is completely independent of θ in S_{in}-S_{out}.

To test this prediction, as noted in the main text we performed room temperature RA-SHG measurements on $1T$-TaS_2 at $\theta = 10°$ and $\theta = 0°$, and obtain a clear θ dependence of the rotational anisotropy. This is a unique feature of electric quadrupole SHG and strongly suggests that part of our signal in Fig. 4 is due to a bulk electric quadrupole contribution.

Having established that the bulk electric quadrupole contribution is present in our SHG signal, we proceed to calculate the value of $\mathscr{I}^{(3)}_{SS}$ and show that it is zero in the presence of vertical mirror plane symmetry. In the text, we use this fact to argue that vertical mirror symmetry is broken in the IC phase of $1T$-TaS_2.

To examine the symmetry properties of $I^{(3)}_{SS}$, we compute the rotational anisotropy in the presence of $Q_{ij}(2\omega)$ as

$$I^{2\omega}_{SS}(\phi) = \left| \left(\bar{\chi}^S_{yjk}(\phi) + 2i\bar{\chi}^Q_{ypjk}(\phi) k_p \right) E_j(\omega) E_k(\omega) \right|^2, \tag{S17}$$

where

$$\bar{\chi}^S_{ijk}(\phi) = R(\phi)_{il} R(\phi)_{jm} R(\phi)_{kn} \chi^S_{lmn}, \tag{S18}$$

$$\bar{\chi}^Q_{ipjk}(\phi) = R(\phi)_{il} R(\phi)_{pq} R(\phi)_{jm} R(\phi)_{kn} \chi^Q_{lqmn}, \tag{S19}$$

and $\boldsymbol{E}(\omega) = (0,1,0)^T$. It is then trivial to compute the Fourier spectrum of $I^{2\omega}_{SS}$. Let χ^S_{ijk} be the surface electric dipole susceptibility tensor constrained by the point group C_3, and let χ^Q_{ijkl} be the bulk electric quadrupole susceptibility tensor constrained by the point group S_6. These point groups correspond to the accepted surface and bulk structures in the NC phase of $1T$-TaS_2 according to x-ray diffraction[6]. Then, we find

$$\mathscr{I}^{(3)}_{SS} = 2\sin\theta\cos\theta \sqrt{\left(\chi^Q_{xzxy}\right)^2 + \left(\chi^Q_{xzyy}\right)^2}. \tag{S20}$$

where $\mathscr{I}^{(3)}_{SS}$ is the 3ϕ Fourier component of the rotational anisotropy in the S_{in}-S_{out} polarization channel.

There are three aspects of Eq. S20 which deserve attention. For one thing, we find that at normal incidence ($\theta = 0$), $\mathscr{I}^{(3)}_{SS} = 0$. This is consistent with the measurements shown in Fig. 4(b). Second, we find that $\mathscr{I}^{(3)}_{SS}$ depends only on the quadrupole susceptibility tensor, which is consistent with the notion that for purely electric dipole $I^{2\omega}_{SS}$ must be symmetric under $\phi \to \phi + \pi$.

The third and most important aspect of Eq. S20 is that, if we promote the symmetry group of the bulk of the sample from S_6 to D_{3d}, which corresponds to restoring the vertical mirror plane symmetry, χ^Q_{xzxy} and χ^Q_{xzyy} become zero[1]. Thus we find that a nonzero value for $\mathscr{I}^{(3)}_{SS}$ is not allowed in D_{3d}, which is the point group of the undistorted phase[6]. Because our measurements in the IC phase (Fig. 4(c)) indicate a nonzero $\mathscr{I}^{(3)}_{SS}$, this suggests that the point group in the IC phase of $1T$-TaS_2 is not D_{3d}, but rather a proper subgroup of D_{3d}. The highest-symmetry proper subgroup of D_{3d} which reasonably fits the data is S_6, which breaks vertical mirror plane symmetry. Note that this is a statement of the bulk point group only; the negligible value of $I^{(3)}_{PS}$ in the IC phase

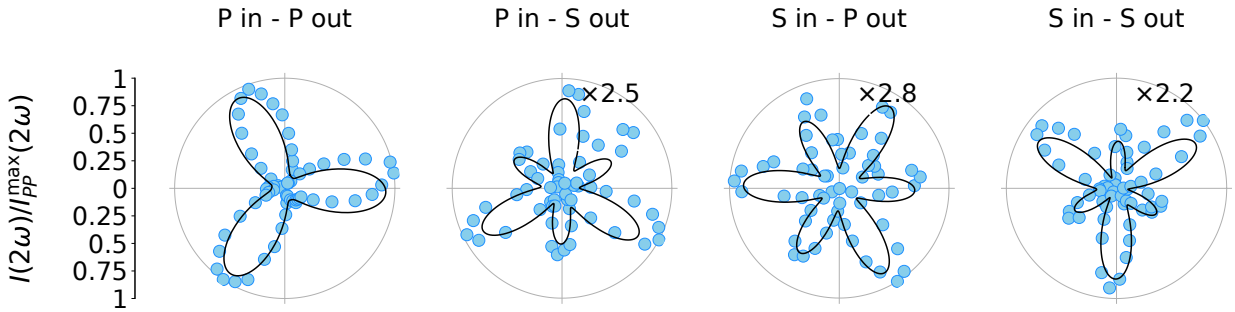

FIG. S5. RA-SHG intensity as a function of ϕ at $T = 295K$. Solid lines are best fits to the data using a surface electric dipole term in the point group C_3, as well as a bulk electric quadrupole term in the point group S_6. Data is normalized to the maximum value of the P_{in}-P_{out} signal.

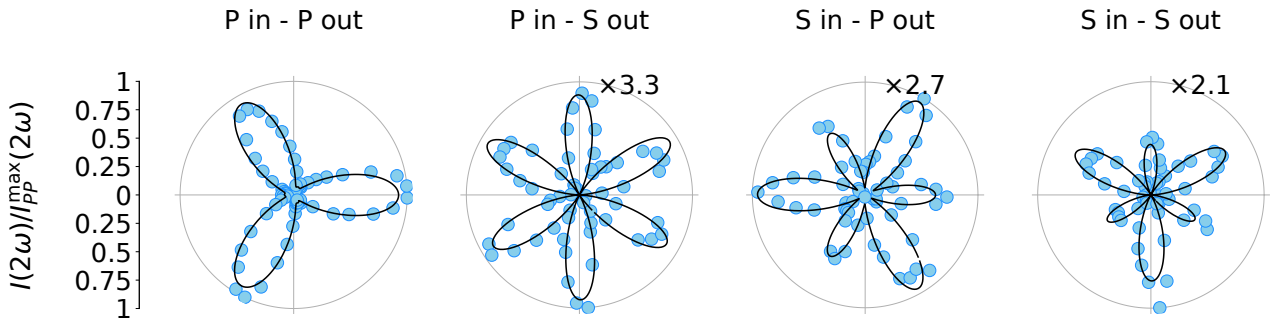

FIG. S6. RA-SHG intensity as a function of ϕ at $T = 356K$. Solid lines are best fits to the data using a surface electric dipole term in the point group C_{3v}, as well as a bulk electric quadrupole term in the point group S_6. Data is normalized to the maximum value of the P_{in}-P_{out} signal.

(Fig. 2) suggests a surface point group of C_{3v}, which retains vertical mirror plane symmetry. This is consistent in the limit where the coupling between the layers is very small, and the separation of surface and bulk contributions to the SHG signal is well-justified.

For the sake of completeness, we also note here two alternative explanations for the nonzero $I_{SS}^{(3)}$ depicted in Fig. 4(c) which do not appeal to an additional quadrupole contribution. Firstly, it is possible that the surface of the sample was rough or nonuniform in such a way as to modulate the observed SHG intensity as a function of ϕ. In principle, this could result in a nonzero observed value of $I_{SS}^{(3)}$. To account for this artifact, we measured SHG on $1T$-TaS_2 in multiple locations and on multiple different samples, and found that the results in this work were consistent across all measurements. Furthermore, with SHG measurements there is always the possibility of an additional contribution arising from the presence of adsorbates on the sample surface[7]. While such a contribution may be present in our experiment, we note that this too is an unlikely explanation for the nonzero $I_{SS}^{(3)}$ because of the wavevector dependence of Figs. 4(a) and (b). This is because the dominant contribution from adsorbates is generally of the electric dipole type and therefore should not depend on $\boldsymbol{k}$ in S_{in}-S_{out}.

* gedik@mit.edu

[1] R. Boyd, *Nonlinear Optics*, 3rd ed. (Academic Press, 2008).
[2] A. Zong, X. Shen, A. Kogar, L. Ye, C. Marks, D. Chowdhury, T. Rohwer, B. Freelon, S. Weathersby, R. Li, J. Yang, J. Checkelsky, X. Wang, and N. Gedik, Science Advances **4** (2018), 10.1126/sciadv.aau5501.
[3] J. Wilson, F. Di Salvo, and S. Mahajan, Advances in Physics **24**, 117 (1975).
[4] M. Bovet, D. Popovi, F. Clerc, C. Koitzsch, U. Probst, E. Bucher, H. Berger, D. Naumovi, and P. Aebi, Physical Review B **69** (2004), 10.1103/PhysRevB.69.125117.
[5] K. N. H. Shiba, in *Structural Phase Transitions in Layered Transition Metal Compounds*, edited by K. Motizuki (D. Reidel Publishing Company, 1986) pp. 175–266.
[6] A. Spijkerman, J. L. de Boer, A. Meetsma, G. A. Wiegers, and S. van Smaalen, Physical Review B **56**, 13757 (1997).
[7] G. Berkovic, Y. R. Shen, G. Marowsky, and R. Steinhoff, J. Opt. Soc. Am. B **6**, 205 (1989).